engineering proceedings

MDPI

Proceeding Paper

Machine Learning Based Real-Time Photoacoustic Surface Crack Detection †

Abdulrhman Alshaya *, Ghadah Alabduljabbar and Asem Alalwan

King Abdulaziz City for Science and Technology (KACST), Riyadh 12354, Saudi Arabia; email1@email.com (G.A.); email2@email.com (A.A.)

* Correspondence: aaalshaya@kacst.edu.sa

† Presented at the 4th International Electronic Conference on Applied Sciences, 27 October–10 November 2023; Available online: https://asec2023.sciforum.net/.

Abstract: Photoacoustic imaging is commonly utilized in biomedical research due to its capability to provide functional and structural details for imaging targets, featuring optical contrast and ultrasound resolution. This imaging technique has also found applications in industry, particularly in non-destructive testing, such as surface crack detection. However, the cost of photoacoustic systems and the time required for scanning and image reconstruction limit their use in non-destructive testing. In this study, a low-cost photoacoustic equipment, combined with machine learning techniques, was applied to surface crack detection. This scanning technique achieved a 97% offline prediction accuracy. Additionally, it demonstrated a reduction in system complexity compared to traditional photoacoustic imaging techniques. This reduction in complexity results from using a single scanning line as input to the machine learning model, unlike the imaging technique, which requires multiple scanning lines for reconstructing the photoacoustic image.

Keywords: photoacoustic; ultrasound; crack; non-destructive testing; industry; machine learning; Convolutional Neural Network

Citation: Alshaya, A.; Alabduljabbar, G.; Alalwan, A. Machine Learning Based Real-Time Photoacoustic Surface Crack Detection. *Eng. Proc.* **2023**, *52*, 0. https://doi.org/

Academic Editor: Firstname Lastname

Published:

1. Introduction

Over the last decades, numerous researchers have explored fracture analysis to enhance material inspection techniques. Cracks in materials comes from product defects, environmental influences like corrosion and fatigue [1], signify structural vulnerability [2]. Material cracking is a known contributor to mechanical system failure in transportation research [3]. Various approaches have been devised, including strain gauges, visual cameras, thermography, and others [4–7]. These techniques primarily rely on employing and observing the same modality; for example, visual cameras utilize optical perturbations and optical observation.

Photoacoustic measurement has emerged as a promising alternative to optical imaging, addressing issues such as diffuse reflection from irregular surfaces [8]. This unique approach employs optical disturbance but captures its effects acoustically, minimizing optical analysis challenges related to scattering effects. While photoacoustic measurement dates back to the 1800s, its complexity slowed the widespread adoption [9]. However, advancements in semiconductor and laser technology in the 1960s have transformed it into a cutting-edge imaging technique [10]. Thus, it is widely utilized in the medical field [11–13]. Researchers have also reported successful applications of photoacoustic measurement in detecting material cracks [14–16]. However, the cost of photoacoustic system, and the time consumption for scanning and imaging reconstruction limits using it in non-destructive testing. Therefore, in this study, low-cost photoacoustic equipment with machine learning technique will be investigated in surface crack detection. This investigation reduces the system complexity and the time consumption for detection compared with that when photoacoustic imaging techniques is used.

2. Method

2.1. Delay and Sum (DAS) Beamforming Technique

Delay and sum (DAS) beamformer is one of the simplest and most popular beamforming technique in ultrasound and photoacoustic imaging. In this beamforming technique, the photoacoustic image is reconstructed based on combining the delayed photoacoustic signals as shown in Equation (1) [17,18]:

$$Y_{DAS} = \sum_{i=1}^{N} RF_i(t, \Delta t), \quad (1)$$

where, Y_{DAS} is the beamformer output, N is the number of transducer elements or scanning lines, $RF_i(t, \Delta t)$ is the delayed photoacoustic signal that is received by element or scanning line number i, and Δt is the time delay.

2.2. Machine Learning Model

The Convolutional Neural Networks (CNN) model architecture used is illustrated in Figure 1. The first layer performs a convolution over the input spectrogram image with 32 kernels size 3 × 3, accompanied by Rectified Linear Unit (ReLU) [19] activation function. The obtained feature maps are then sub-sampled using a max-pooling layer operating over 2 × 2 squares. The second and third convolutional layers are the same as the first one except they have higher number of kernels (64 and 128 respectively). The last sub-sampling operation is max-pooling layer which operates over the entire sequence length. A batch normalization [20] was used as an intermediate layer after each convolutional layer. For regularization we added a dropout layer equal to 0.5 after the last max-pooling layer. Finally, to classify the spectrogram image to see if it obtained from a cracked or uncracked place, the output layer consists of a fully connected layer with a sigmoid activation function.

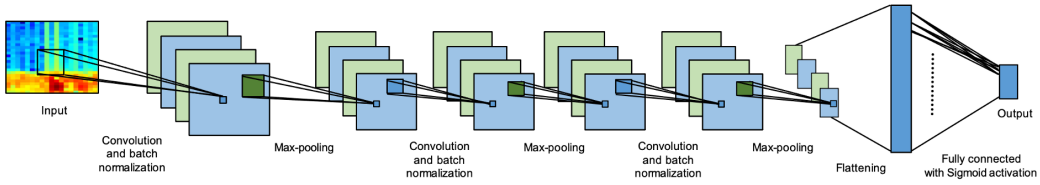

Figure 1. A flow-diagram of the CNN model architecture.

3. Experiment Setup

In this experiment, photoacoustic emissions were generated from a piece of black plastic with four surface cracks that is shown in Figure 2B. The width of each crack was almost 1mm. The photoacoustic emissions were generated from this phantom using a pulse laser diode (PLD) (905D5S3J08X). The pulse width of each firing laser pulse was 100 nm. In addition, the output optical energy and wavelength of this PLD were 3 μJ and 905 nm, respectively. In this experiment, photoacoustic emissions were acquired by using an open-source ultrasound board [21] with one element ultrasound transducer (C310-SU). The centre frequency and bandwidth of this transducer were 5MHz and 90% of the centre frequency, respectively. The scanning step of the ultrasound transducer in the lateral direction was 0.1 mm. The received photoacoustic emission for each scanning point was averaged 10 times before using it to improve its SNR. Figure 2A,C show the schematic diagram of experiment setup and real photo for experiment, respectively. In this experiment, 1131 photoacoustic signals were acquired from a cracked place and 4522 photoacoustic signals were acquired from an uncracked place. These received signals were converted to spectrogram images before using them in the machine learning model. In this study, a CNN classification model was used for detecting the presence of cracks in the surfaces. The dataset was randomly split into two independent parts with 80% and 20% for training and testing, respectively.

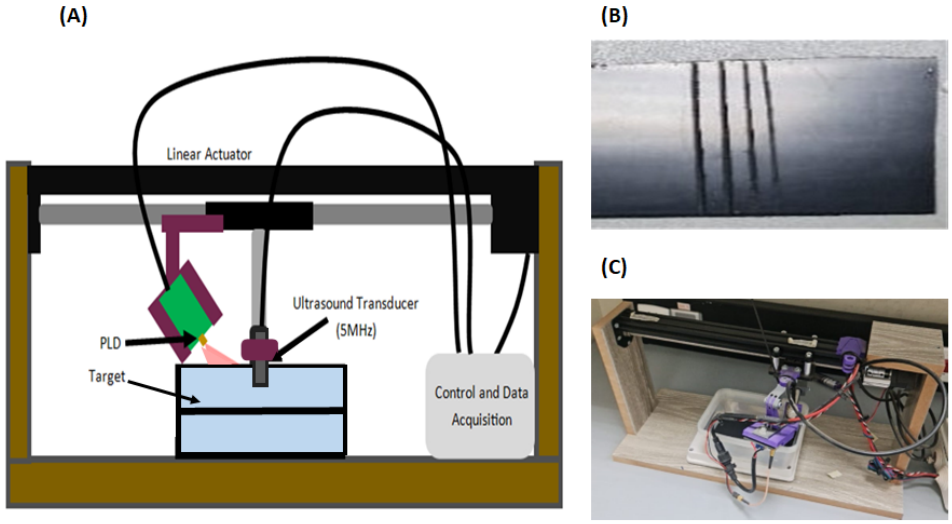

Figure 2. (**A**) Schematic diagram of experiment setup, (**B**) A piece of black plastic with four surface cracks, and (**C**) Experiment setup.

4. Results and Discussion

The received photoacoustic signals from black plastic with four surface cracks was beamformed by using DAS beamformer as shown in Figure 3. The FIR bandpass filter (2.5–7.5 MHz) with Hamming window were used in this beamformer. From Figure 3, the place of surface cracks can be clearly defined compared with uncracked place. In this experiment, 5653 photoacoustic signals are acquired. 1131 of these signals were acquired from a cracked place and 4522 of these signals were acquired from an uncracked place. These received signals were converted to spectrogram images before using them in the machine learning model. In this conversion, the segment length was 100 samples, the window type was hamming window, and the length of overlap window was 50 samples. An example for cracked and un-cracked images are shown in Figure 4.

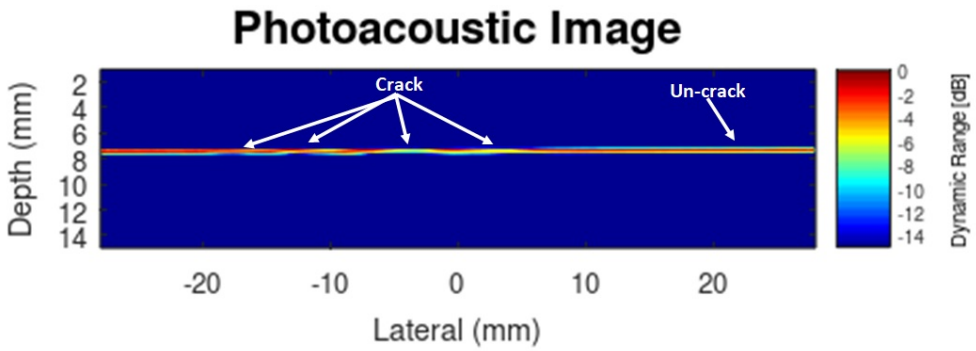

Figure 3. Photoacoustic image for black plastic with four surface cracks.

The CNN model was implemented using the Keras Python library. To validate the performances of the model, the data set was randomly divided into two independent sets 80% for training, and 20% for testing. The binary cross-entropy loss function and the Adaptive Momentum (ADAM) [22] optimization approach with decay rate $\beta 1 = 0.9$, $\beta 2 = 0.999$, and learning rate = 0.001 were utilized. The batch size was set to 32, and the number of epochs for the training process is 50 with early stopping condition in case there was no improvements over 10 epochs. After the process of training and validating the model, the model yielded a loss of 0.121, and accuracy of 97%, and F1 score of 91.38%. The confusion matrix that was used to calculate the performances of the model is presented in Figure 5. From this figure, it can be noted that the model correctly classified all images in the testing set that was acquired from an uncracked place, while missed to classified

15.9% of the images that was acquired from a cracked place (33 images out of 208). This percentage of missing was due to imbalanced between cracks and uncracks that were used to train the machine learning model.

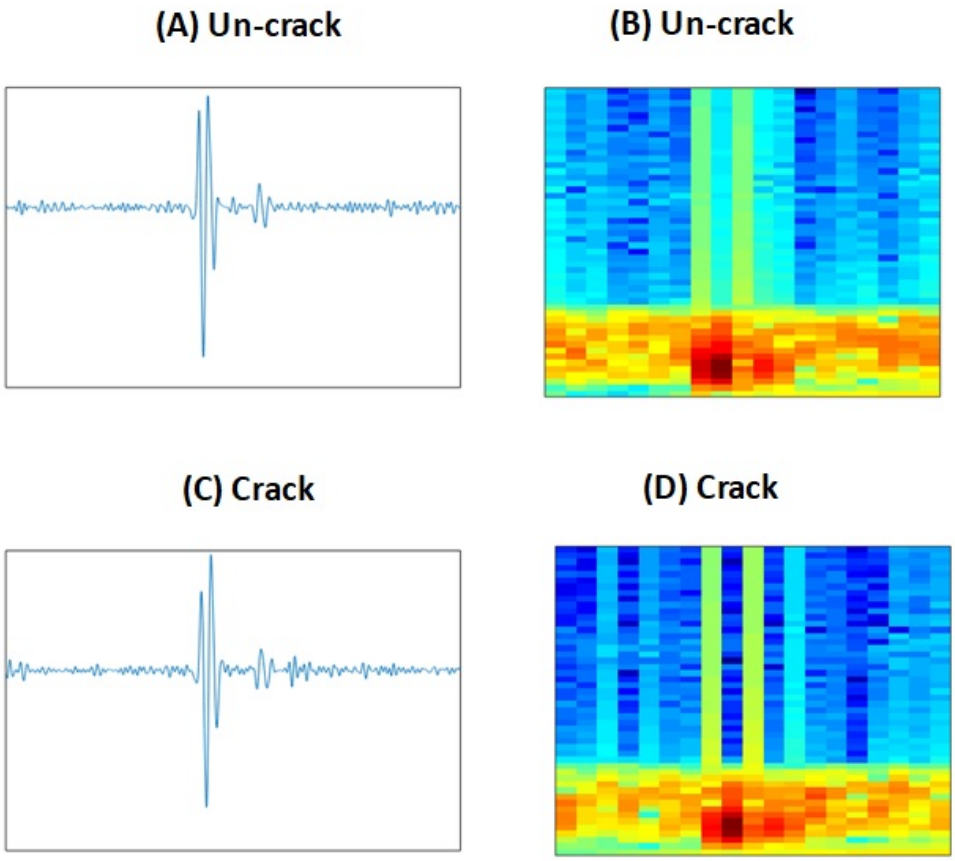

Figure 4. (**A**) Un-cracked photoacoustic signal, (**B**) Un-cracked photoacoustic spectrogram image, (**C**) Cracked photoacoustic signal, and (**D**) Cracked photoacoustic spectrogram image.

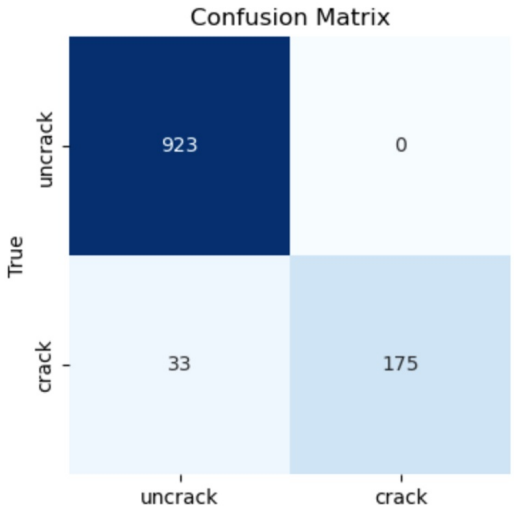

Figure 5. Confusion matrix summary.

When comparing this machine learning detection technique with the image reconstruction technique, the machine learning technique reduced the complexity of the system. This is because one scanning line is used as input to the machine learning model, unlike

the imaging technique that needs multiple scanning lines to reconstruct the photoacoustic image. For instance, to detect and image a single surface crack in this experiment, almost 20 scanning lines are needed to acquire. This results in consuming time and memory. The number of scanning lines that are needs to imaging single crack could be increased depends on the distance between imaging target and focus point of ultrasound transducer, the size of scanning step, and the minimum size of the target crack. In addition, cracks with different level can be easily detect using machine learning technique. This is unlike the imaging reconstruction technique that is affected by the contrast level of the imaging targets. For example, in Figure 3, it is difficult to discover the four cracks at the same time. This is because the large contrast difference between cracks.

5. Conclusions

In this paper, the surface crack was detected by using photoacoustic technology with machine learning. The offline prediction accuracy of surface crack detection model was 97%. The machine learning detection technique reduced the system complexity and computation time when compared with image reconstruction technique. In future work, the training data for the machine learning model will be balanced to reduce the percentage of classification missing. The machine learning model will be also developed to detect the internal and surface cracks.

Author Contributions: text

Funding: text

Institutional Review Board Statement: text

Informed Consent Statement: text

Data Availability Statement: text

Conflicts of Interest: text

References

1. Konsta-Gdoutos, M.; Gdoutos, E. The effect of load and geometry on the failure modes of sandwich beams. *Appl. Compos. Mater.* **2005**, *12*, 165–176.
2. Bouayoune, K.S.; Boudi, E.M.; Bachir, A. A stochastic method based on the Markov Model of unit jump for analyzing crack jump in a material. *Int. J. Technol.* **2017**, *8*, 622–633.
3. Craig, R.R., Jr.; Kurdila, A.J. *Fundamentals of Structural Dynamics*; John Wiley & Sons: Hoboken, NJ, USA, 2006.
4. Tolev, J.; Mandelis, A. Laser photothermal non-destructive inspection method for hairline crack detection in unsintered automotive parts: A statistical approach. *Ndt Int.* **2010**, *43*, 283–296.
5. Lantz, G.A. Crack Detection Using a Passive Wireless Strain Sensor. Ph.D. Thesis, Georgia Institute of Technology, Atlanta, GA, USA, 2011.
6. Rupil, J.; Roux, S.; Hild, F.; Vincent, L. Fatigue microcrack detection with digital image correlation. *J. Strain Anal. Eng. Des.* **2011**, *46*, 492–509.
7. Jeong, W.; Earls, C.; Philpot, W.; Zehnder, A. Inverse thermographic characterization of optically unresolvable through cracks in thin metal plates. *Mech. Syst. Signal Process.* **2012**, *27*, 634–650.
8. Tam, A.C. Applications of photoacoustic sensing techniques. *Rev. Mod. Phys.* **1986**, *58*, 381.
9. Wang, L.V. *Photoacoustic Imaging and Spectroscopy*; CRC Press: Boca Raton, FL, USA, 2017.
10. Ganguly, P.; Rao, C. Photoacoustic spectroscopy of solids and surfaces. *J. Chem. Sci.* **1981**, *90*, 153–214.
11. Alshaya, A.; Harput, S.; Moubark, A.M.; Cowell, D.M.J.; McLaughlan, J.; Freear, S. Spatial resolution and contrast enhancement in photoacoustic imaging with filter delay multiply and sum beamforming technique. In Proceedings of the 2016 IEEE International Ultrasonics Symposium (IUS), Tours, France, 18–21 September 2016; pp. 1–4. https://doi.org/10.1109/ULTSYM.2016.7728682.
12. Alshaya, A.; Nie, L.; Cowell, D.M.J.; Carpenter, T.; McLaughlan, J.R.; Freear, S. Monitoring Needle Biopsy of Sentinel Lymph Nodes Using Photoacoustic Image with Dynamic-FDMAS Beamformer. In Proceedings of the 2019 IEEE International Ultrasonics Symposium (IUS), Glasgow, UK, 6–9 October 2019; pp. 490–493. https://doi.org/10.1109/ULTSYM.2019.8926274.
13. Sivasubramanian, K.; Periyasamy, V.; Pramanik, M. Non-invasive sentinel lymph node mapping and needle guidance using clinical handheld photoacoustic imaging system in small animal. *J. Biophotonics* **2018**, *11*, e201700061.
14. Mezil, S.; Chigarev, N.; Tournat, V.; Gusev, V. Two dimensional nonlinear frequency-mixing photo-acoustic imaging of a crack and observation of crack phantoms. *J. Appl. Phys.* **2013**, *114*, 174901.

15. Yan, L.; Gao, C.; Zhao, B.; Ma, X.; Zhuang, N.; Duan, H. Non-destructive imaging of standard cracks of railway by photoacoustic piezoelectric technology. *Int. J. Thermophys.* **2012**, *33*, 2001–2005.
16. Chigarev, N.; Zakrzewski, J.; Tournat, V.; Gusev, V. Nonlinear frequency-mixing photoacoustic imaging of a crack. *J. Appl. Phys.* **2009**, *106*, 036101.
17. Yoon, C.; Kang, J.; Han, S.; Yoo, Y.; Song, T.K.; Chang, J.H. Enhancement of photoacoustic image quality by sound speed correction: ex vivo evaluation. *Opt. Express* **2012**, *20*, 3082–3090.
18. Liao, C.K.; Li, M.L.; Li, P.C. Optoacoustic imaging with synthetic aperture focusing and coherence weighting. *Opt. Lett.* **2004**, *29*, 2506–2508.
19. Glorot, X.; Bordes, A.; Bengio, Y. Deep sparse rectifier neural networks. In Proceedings of the Fourteenth international Conference on Artificial Intelligence and Statistics, JMLR Workshop and Conference Proceedings, Fort Lauderdale, FL, USA, 11–13 April 2011; pp. 315–323.
20. Ioffe, S.; Szegedy, C. Batch normalization: Accelerating deep network training by reducing internal covariate shift. In Proceedings of the International Conference on Machine Learning, PMLR, Lille, France, 7–9 July 2015; pp. 448–456.
21. Jonveaux, L. un0rick: Open-source fpga board for single element ultrasound imaging. *Zenodo* **2019**. https://doi.org/10.5281/zenodo.3364559.
22. Kingma, D.P.; Ba, J. Adam: A method for stochastic optimization. *arXiv* **2014**, arXiv:1412.6980.